

Electronic Supplementary Information

New multifunctional 3D porous metal-organic framework with selective gas adsorption, efficient chemical fixation of CO₂ and dye adsorption

Shan Cheng, Yunlong Wu, Jing Jin, Jiao Liu, Dan Wu, Guoping Yang* and Yao-Yu Wang

Key Laboratory of Synthetic and Natural Functional Molecule Chemistry of the Ministry of Education, Shaanxi Key Laboratory of Physico-Inorganic Chemistry, College of Chemistry & Materials Science, Northwest University, Xi'an 710127, P. R. China

Table S1 Selected bond lengths (Å) and bond angles (°) for **1**.

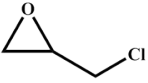
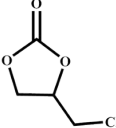
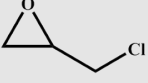
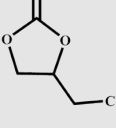
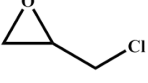
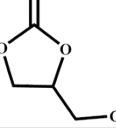
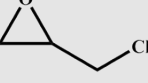
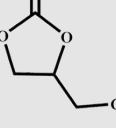
MOF 1			
Mn(1)-O(1)	2.147(4)	O(6)-Mn(2)-O(3)#1	92.12(15)
Mn(1)-O(2)#1	2.160(4)	O(6)-Mn(2)-O(4)	85.20(14)
Mn(1)-O(7)#2	2.116(4)	O(6)-Mn(2)-O(15)	87.71(15)
Mn(1)-O(9)#2	2.188(4)	O(6)-Mn(2)-O(16)#3	102.57(17)
Mn(1)-O(12)	2.247(3)	O(15)-Mn(2)-O(1)	83.64(13)
Mn(1)-O(20)	2.136(4)	O(15)-Mn(2)-O(2)#1	85.58(13)
Mn(2)-O(1)	2.489(4)	O(15)-Mn(2)-O(3)#1	90.25(15)
Mn(2)-O(2)#1	2.367(4)	O(15)-Mn(2)-O(4)	85.00(13)
Mn(2)-O(3)#1	2.282(4)	O(16)#3-Mn(2)-O(1)	88.25(16)
Mn(2)-O(4)	2.333(4)	O(16)#3-Mn(2)-O(2)#1	85.91(15)
Mn(2)-O(6)	2.125(4)	O(16)#3-Mn(2)-O(3)#1	89.82(16)
Mn(2)-O(15)	2.185(4)	O(16)#3-Mn(2)-O(4)	95.30(15)
Mn(2)-O(16)#3	2.140(4)	O(16)#3-Mn(2)-O(15)	169.71(16)
Mn(3)-O(4)	2.248(4)	O(4)-Mn(3)-O(18)#4	89.45(15)

Mn(3)-O(5)	2.104(4)	O(5)-Mn(3)-O(4)	85.54(15)
Mn(3)-O(11)	2.211(5)	O(5)-Mn(3)-O(11)	91.2(2)
Mn(3)-O(17)#3	2.066(4)	O(5)-Mn(3)-O(18)#4	155.08(17)
Mn(3)-O(18)#4	2.357(4)	O(5)-Mn(3)-O(19)#4	99.42(16)
Mn(3)-O(19)#4	2.205(4)	O(11)-Mn(3)-O(4)	173.33(18)
Mn(4)-O(8)#2	2.150(4)	O(11)-Mn(3)-O(18)#4	95.9(2)
Mn(4)-O(9)#2	2.275(4)	O(17)#3-Mn(3)-O(4)	91.20(16)
Mn(4)-O(10)#2	2.342(4)	O(17)#3-Mn(3)-O(5)	110.76(17)
Mn(4)-O(12)	2.215(4)	O(17)#3-Mn(3)-O(11)	84.5(2)
Mn(4)-O(13)	2.141(4)	O(17)#3-Mn(3)-O(18)#4	93.71(16)
Mn(4)-O(14)	2.108(6)	O(17)#3-Mn(3)-O(19)#4	149.08(17)
O(1)-Mn(1)-O(2)#1	83.13(14)	O(19)#4-Mn(3)-O(4)	97.85(16)
O(1)-Mn(1)-O(9)#2	96.20(15)	O(19)#4-Mn(3)-O(11)	88.41(19)
O(1)-Mn(1)-O(12)	87.94(14)	O(19)#4-Mn(3)-O(18)#4	57.10(15)
O(2)#1-Mn(1)-O(9)#2	171.49(15)	O(8)#2-Mn(4)-O(9)#2	92.19(15)
O(2)#1-Mn(1)-O(12)	93.49(14)	O(8)#2-Mn(4)-O(10)#2	83.72(15)
O(7)#2-Mn(1)-O(1)	174.77(16)	O(8)#2-Mn(4)-O(12)	88.54(15)
O(7)#2-Mn(1)-O(2)#1	94.56(15)	O(9)#2-Mn(4)-O(10)#2	56.33(14)
O(7)#2-Mn(1)-O(9)#2	85.40(15)	O(12)-Mn(4)-O(9)#2	76.85(13)
O(7)#2-Mn(1)-O(12)	87.52(15)	O(12)-Mn(4)-O(10)#2	132.02(14)
O(7)#2-Mn(1)-O(20)	92.97(18)	O(13)-Mn(4)-O(8)#2	174.29(18)
O(9)#2-Mn(1)-O(12)	78.00(13)	O(13)-Mn(4)-O(9)#2	91.37(17)
O(20)-Mn(1)-O(1)	91.76(17)	O(13)-Mn(4)-O(10)#2	101.98(16)
O(20)-Mn(1)-O(2)#1	91.0(2)	O(13)-Mn(4)-O(12)	87.92(16)
O(20)-Mn(1)-O(9)#2	97.52(19)	O(14)-Mn(4)-O(8)#2	88.2(2)
O(20)-Mn(1)-O(12)	175.44(19)	O(14)-Mn(4)-O(9)#2	155.4(2)
O(2)#1-Mn(2)-O(1)	72.04(12)	O(14)-Mn(4)-O(10)#2	99.4(2)
O(3)#1-Mn(2)-O(1)	128.23(13)	O(14)-Mn(4)-O(12)	127.7(2)
O(3)#1-Mn(2)-O(2)#1	56.22(13)	O(14)-Mn(4)-O(13)	90.5(2)
O(3)#1-Mn(2)-O(4)	174.63(15)	Mn(1)-O(1)-Mn(2)	96.80(14)

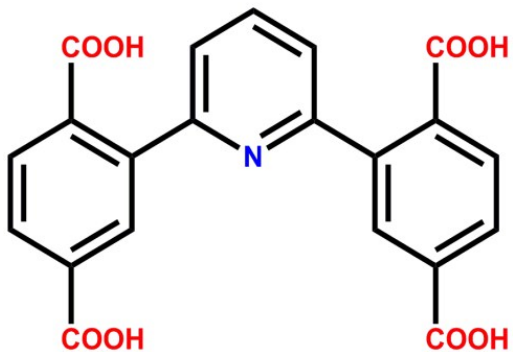
O(4)-Mn(2)-O(1)	53.75(12)	Mn(1)#1-O(2)-Mn(2)#1	100.14(14)
O(4)-Mn(2)-O(2)#1	125.66(13)	Mn(3)-O(4)-Mn(2)	106.79(15)
O(6)-Mn(2)-O(1)	138.56(14)	Mn(1)#5-O(9)-Mn(4)#5	98.34(14)
O(6)-Mn(2)-O(2)#1	147.52(14)	Mn(4)-O(12)-Mn(1)	98.39(13)

Symmetrical codes:#1 -x+2, -y+1, -z+1; #2 x, y-1, z; #3 x+1, y, z; #4 -x+2, -y, -z; #5 x, y+1, z; #6 x-1, y, z.

Table S2 The temperature gradient experiments of the CO₂ cycloaddition catalyzed by MOF 1/TBAB.

Entry	Epoxides	Products	Yield
1			~80%
2			~95%
3			~98%
4			>99%

Reaction condition: 2-(chloromethyl)oxirane (20 mmol); MOF 1 (0.1 mmol); TBAB (2 mmol); dioxygen gas: CO₂ containing balloon; reaction 25 °C for 1; 40 °C for 2; 60 °C for 3; 80 °C for 4; reaction 8 h.



Scheme S1 The structure of ligand 1,3-di(2',4'-dicarboxyphenyl)pyridine (H₄L).

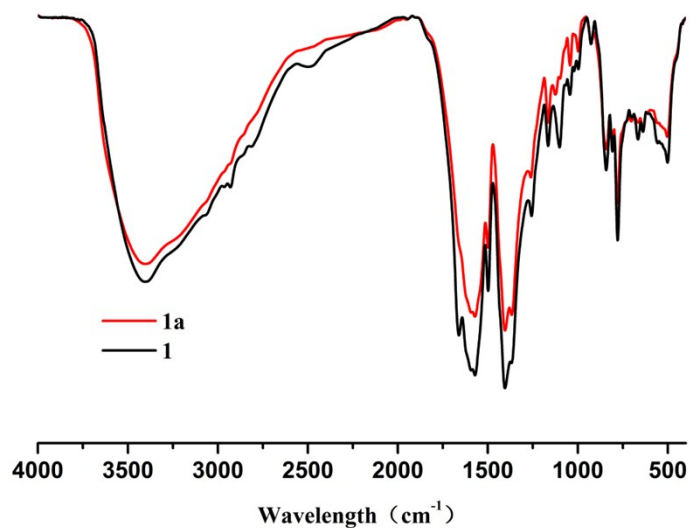


Fig. S1 The FT-IR spectra of complexes **1** and **1a**.

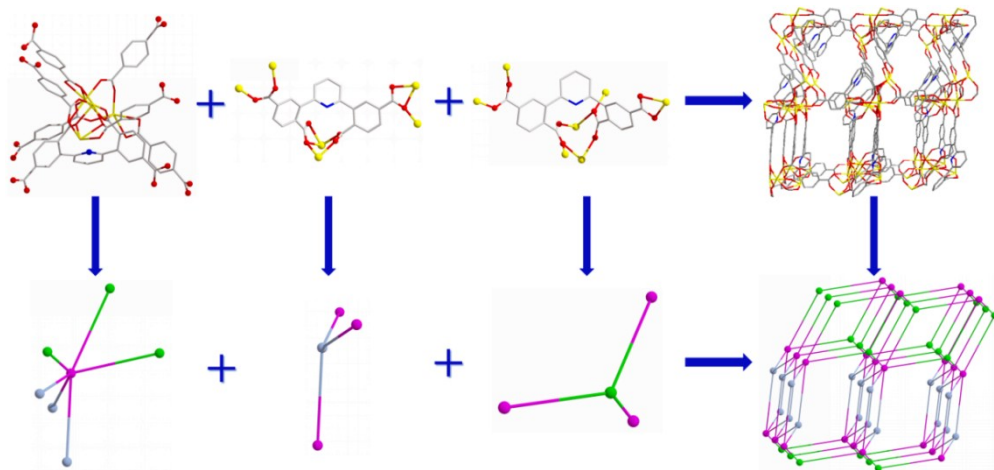


Fig. S2 Topology analysis of **1**, where the 6-connected nodes are the Mn₄ cluster, and the 3-connected nodes are the ligands.

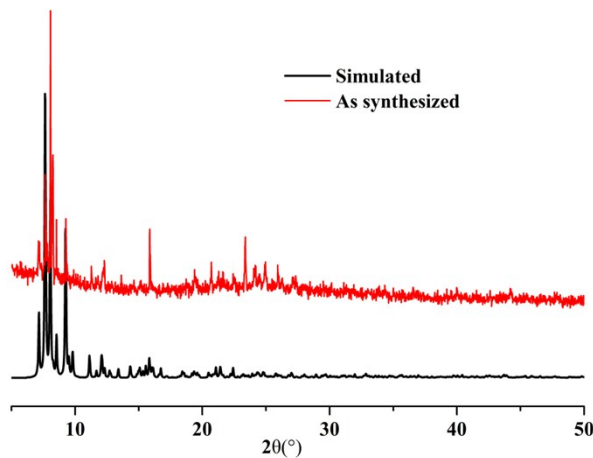


Fig. S3 PXRD patterns of MOF **1** by the simulated from crystal data and new as-synthesized

sample.

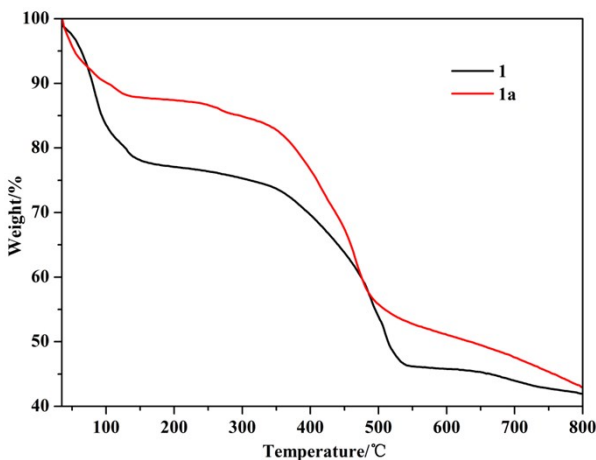


Fig. S4 TGA curves of the as-synthesized **1** and desolvated sample **1a**.

IAST adsorption selectivity calculation

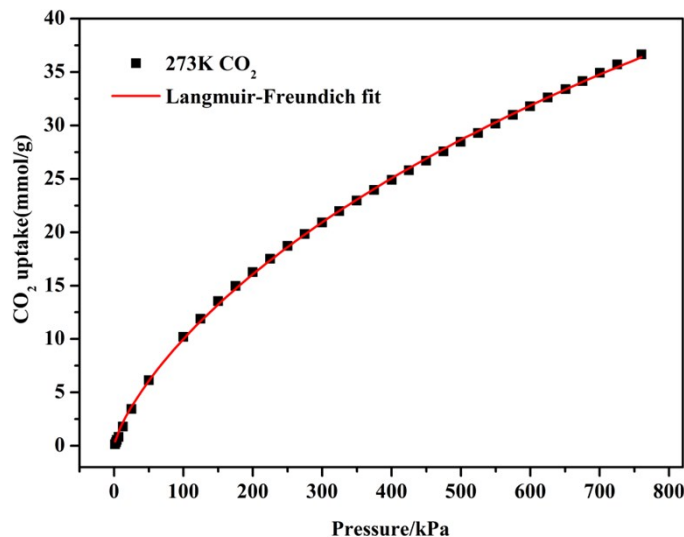
The experimental isotherm data for pure CO₂ and CH₄ (measured at 273 and 298 K) were fitted using a Langmuir-Freundlich (L-F) model

$$q = \frac{a * b * p^c}{1 + b * p^c}$$

Where q and p are adsorbed amounts and pressures of component i , respectively. The adsorption selectivities for binary mixtures of CO₂/CH₄ at 273 and 298 K, defined by

$$S_{ads} = (q_1 / q_2) / (p_1 / p_2)$$

Where q_i is the amount of i adsorbed and p_i is the partial pressure of i in the mixture.



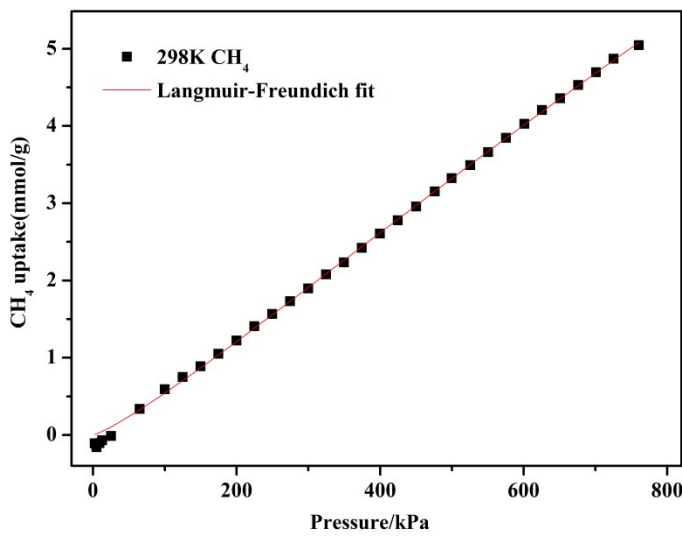
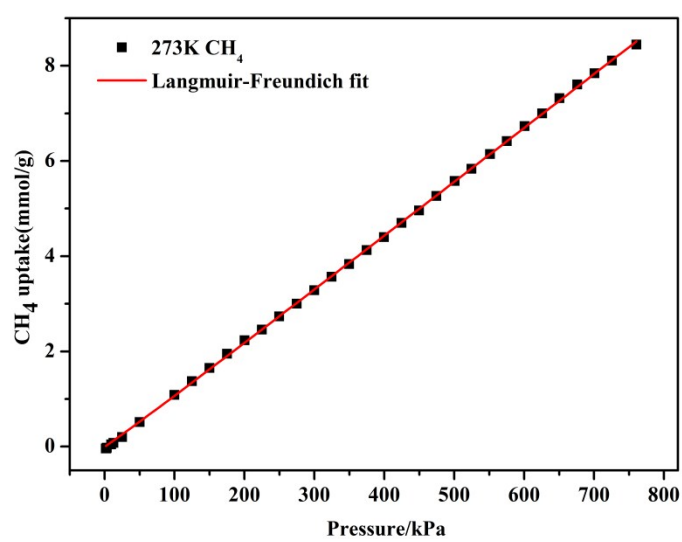
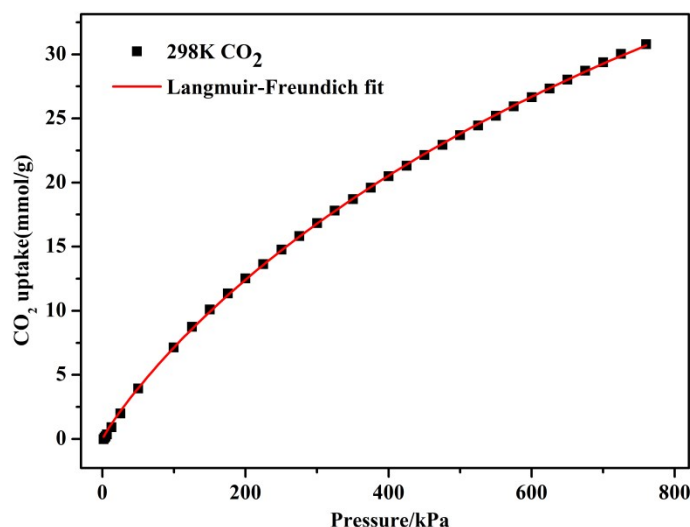


Fig. S5 CO₂ adsorption isotherms of **1a** at 273K with fitting by L-F model: a = 129.55713, b

$= 0.00253$, $c = 0.75972$, $\text{Chi}^2 = 0.04991$, $R^2 = 0.99964$; CO_2 adsorption isotherms of **1a** at 298K with fitting by L-F model: $a = 82.60548$, $b = 0.00147$, $c = 0.90378$, $\text{Chi}^2 = 0.01828$, $R^2 = 0.99982$; CH_4 adsorption isotherms of **1a** at 273K with fitting by L-F model: $a = 367.05928$, $b = 2.50324\text{E-}5$, $c = 1.03326$, $\text{Chi}^2 = 0.00128$, $R^2 = 0.99983$; CH_4 adsorption isotherms of **1a** at 298K with fitting by L-F model: $a = 27.58489$, $b = 8.27566\text{E-}5$, $c = 1.19249$, $\text{Chi}^2 = 0.00335$, $R^2 = 0.99879$.

Calculation of sorption heat for CO_2 uptake using Virial 2 model

$$\square \ln P = \ln N + 1/T \sum_{i=0}^m aiN^i + \sum_{i=0}^n biN^i$$

$$Q_{st} = -R \sum_{i=0}^m aiN^i$$

The above equation was applied to fit the combined CO_2 isotherm data for desolvated **1** at 273 and 298 K, where P is the pressure, N is the adsorbed amount, T is the temperature, ai and bi are virial coefficients, and m and n are the number of coefficients used to describe the isotherms. Q_{st} is the coverage-dependent enthalpy of adsorption and R is the universal gas constant.

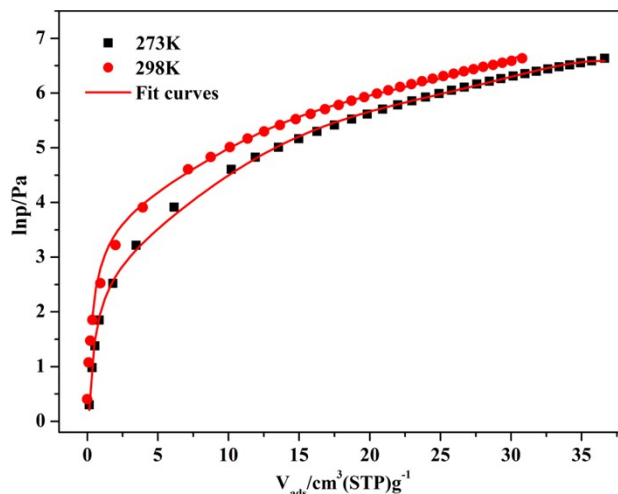


Fig. S6 Virial analysis of the CO_2 adsorption data at 273 and 298 K for **1**. Fitting results: $a_0 = -2766.59447$, $a_1 = 101.41552$, $a_2 = 5.88105$, $a_3 = -0.5561$, $a_4 = 0.01453$, $a_5 = -1.39362\text{E-}4$; $\text{Chi}^2 = 0.01016$, $R^2 = 0.99664$.

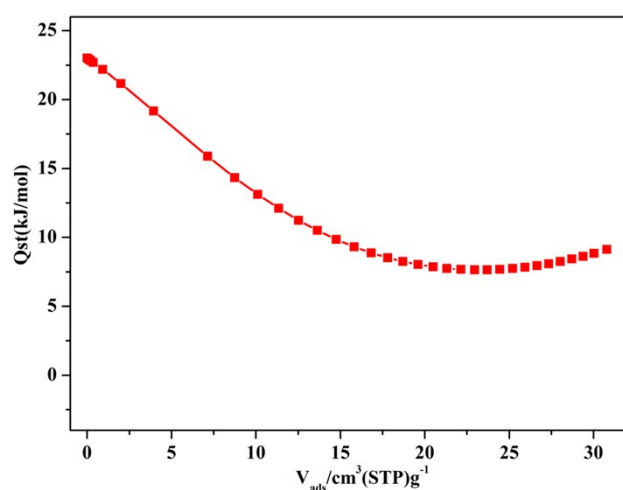
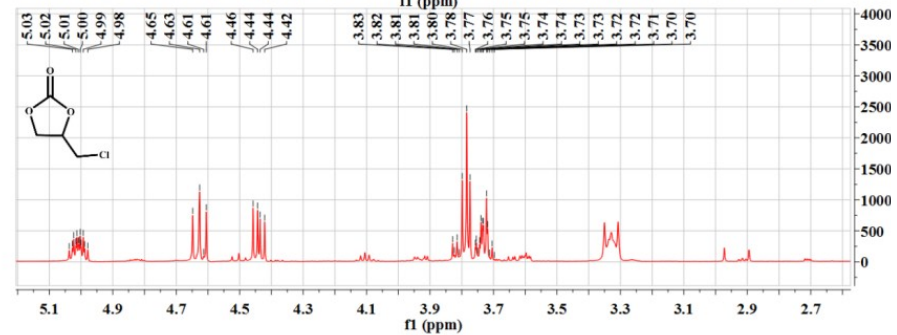
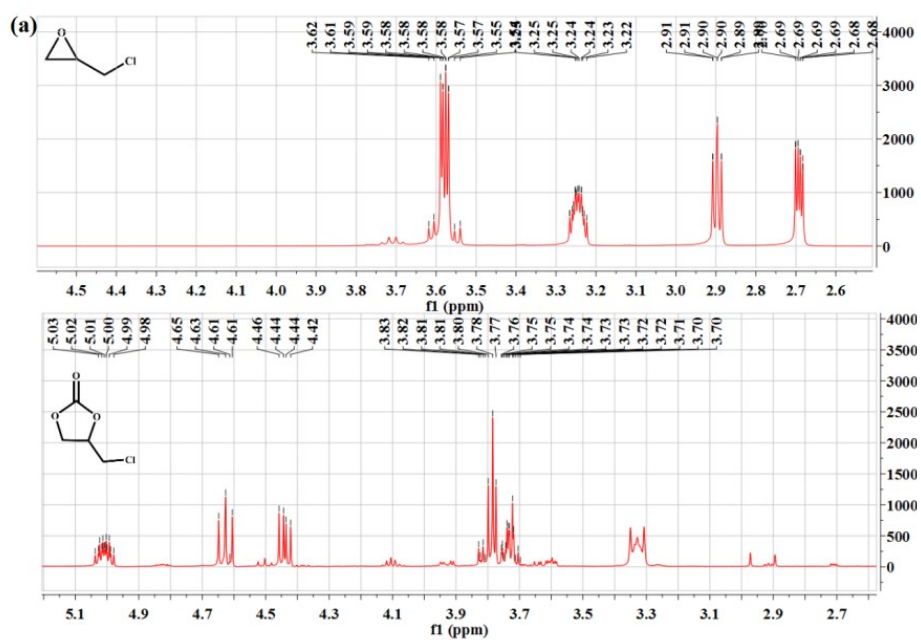
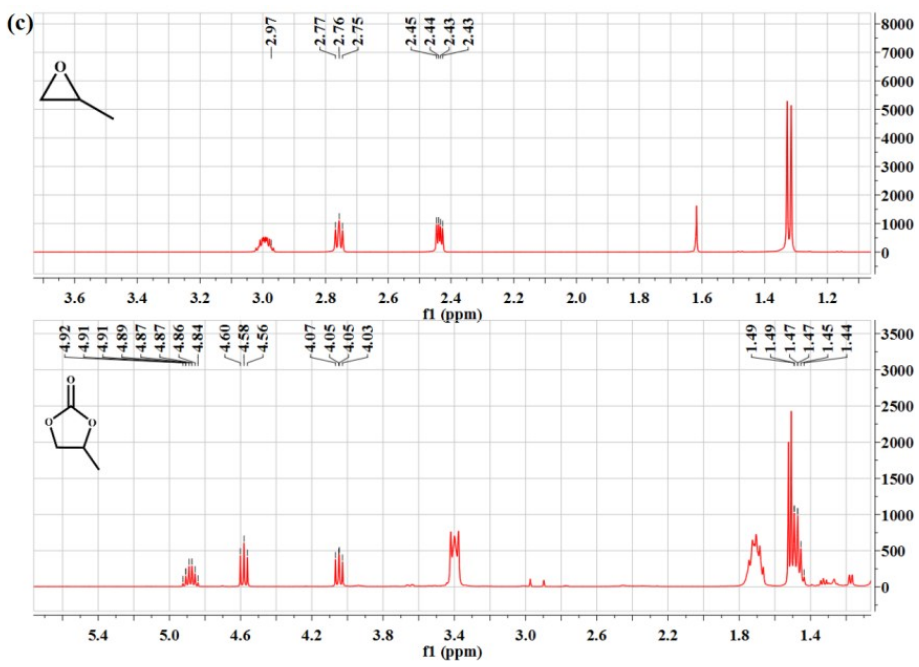
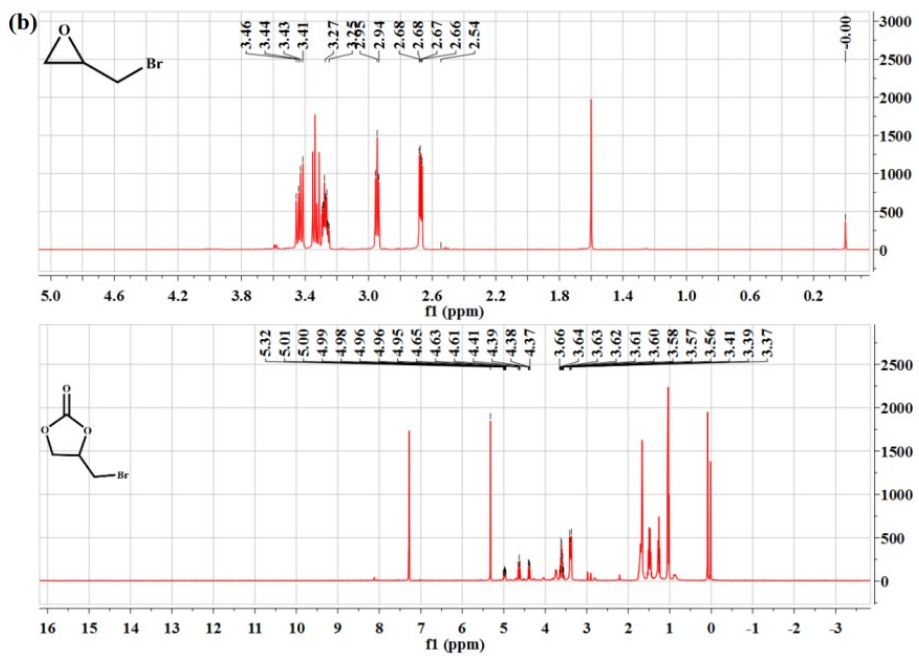
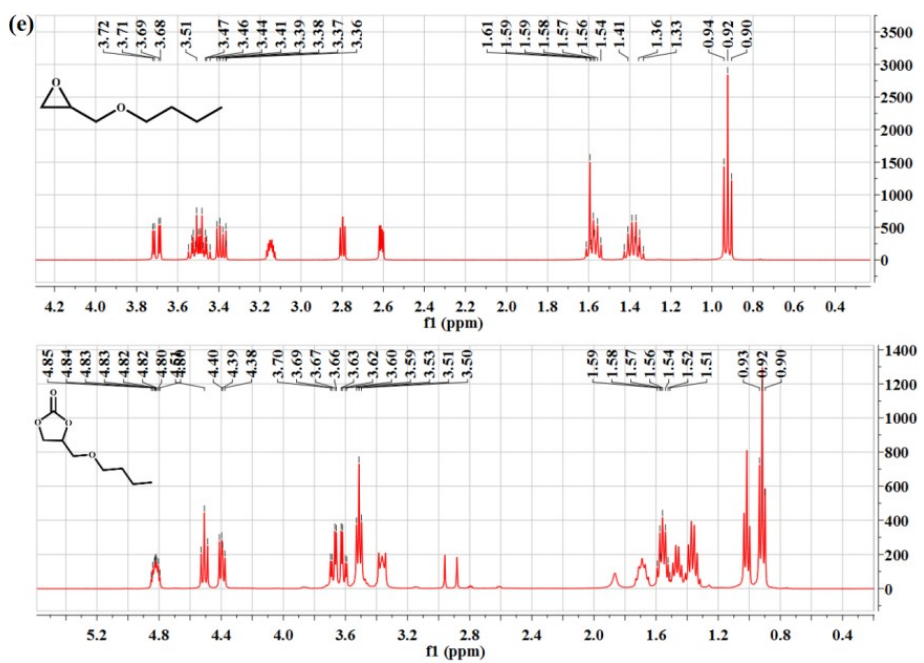
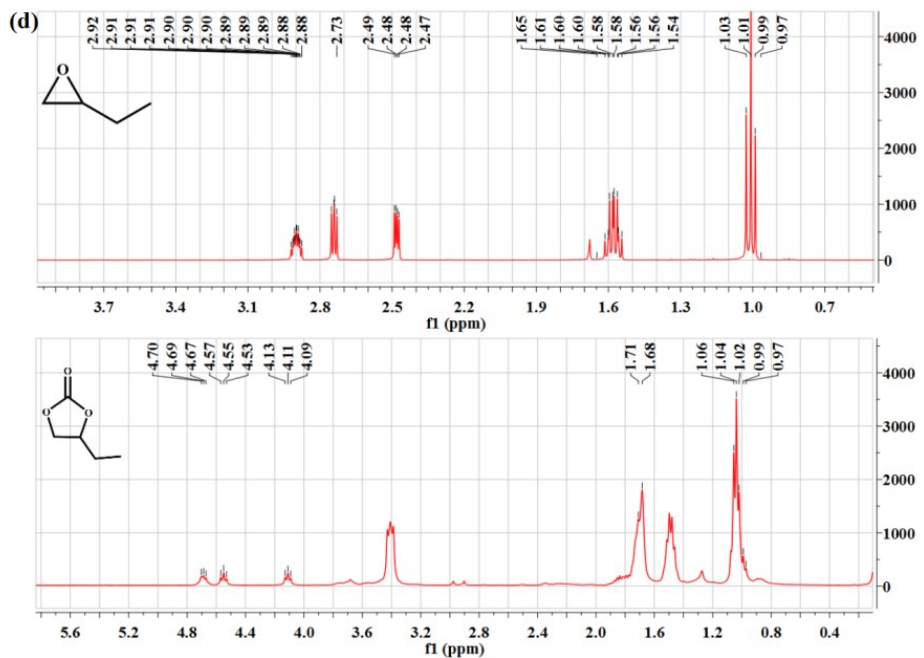


Fig. S7 Isosteric heat of CO_2 adsorption for **1a** estimated by the virial equation from the adsorption isotherms at 273 and 298 K.







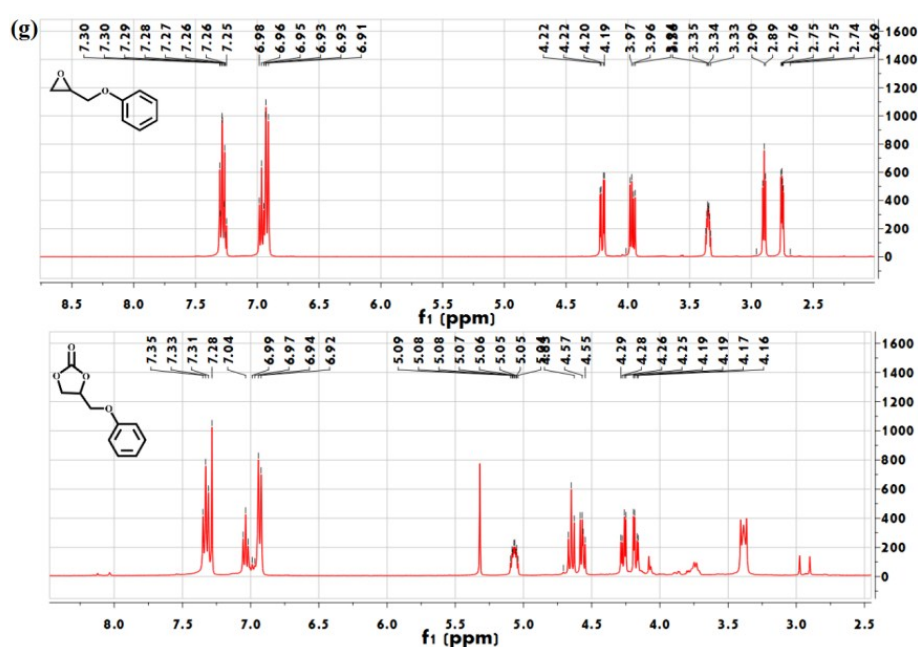
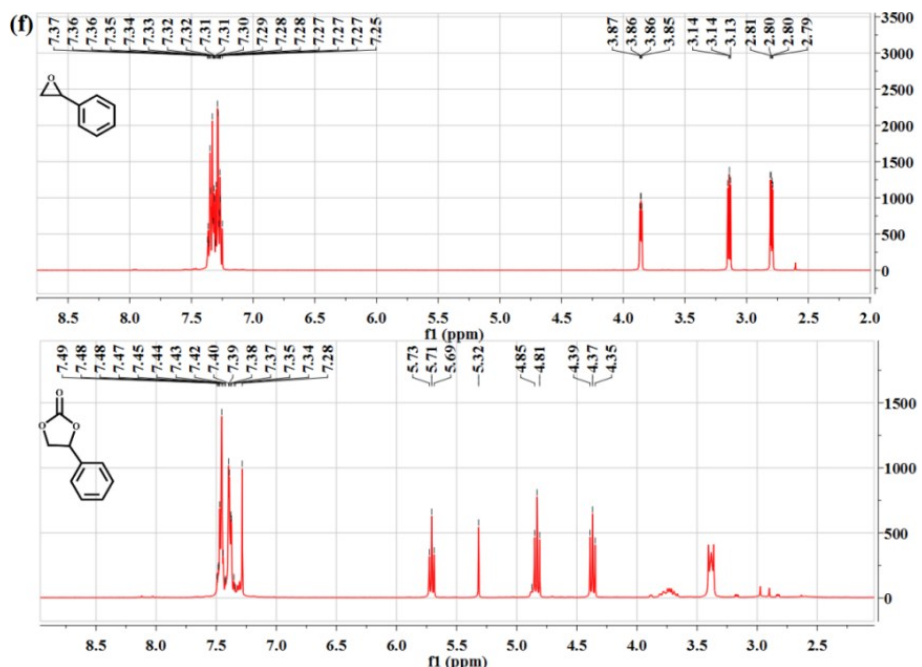


Fig. S8 ^1H NMR spectrum of cyclic carbonate products of (a) 4-chloromethyl-1,3-dioxolan-2-one (b) 4-bromomethyl-1,3-dioxolan-2-one. (c) propylene carbonate. (d) 4-ethyl-1,3-dioxolan-2-one. (e) 3-butoxy-1,2-propylene carbonate. (f) styrene carbonate. (g) 4-(phenoxy)methyl-1,3-dioxolan-2-one in CDCl_3 .

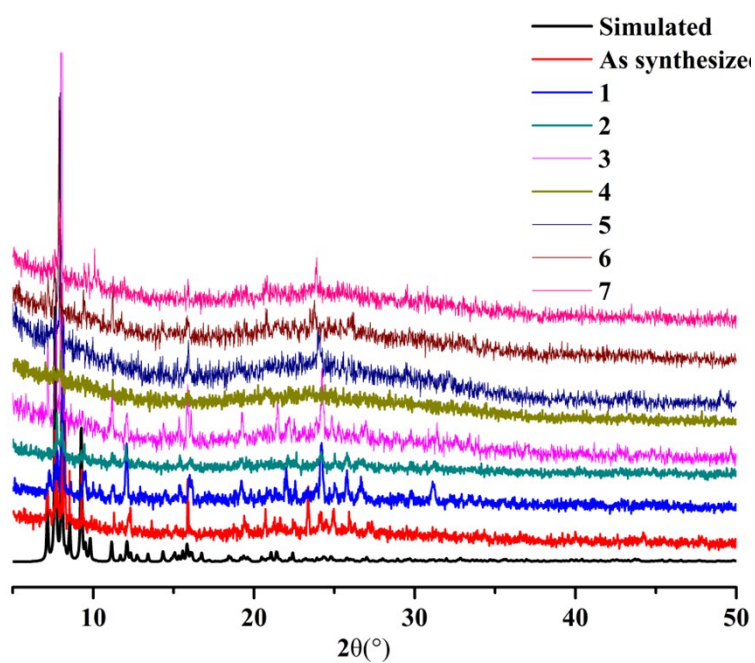


Fig. S9 The PXRD patterns of compound **1** after six catalytic recycling. [**1**: (-CH₂-O-Ph) **2**: (-C₂H₅) **3**: (-CH₃) **4**: (-CH₂-O-C₄H₉) **5**: (-Ph) **6**: (-CH₂-Br) **7**: (-CH₂-Cl)].

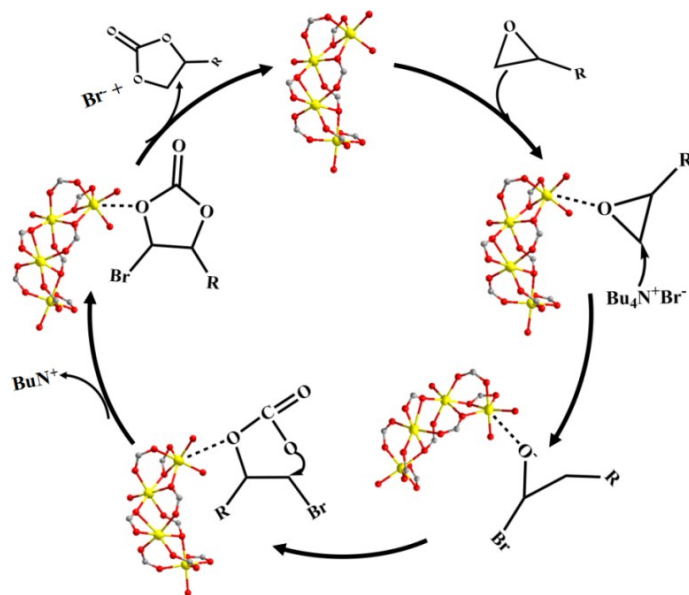


Fig. S10 The possible mechanism for the cycloaddition reaction of epoxides with CO_2 into cyclic carbonates.

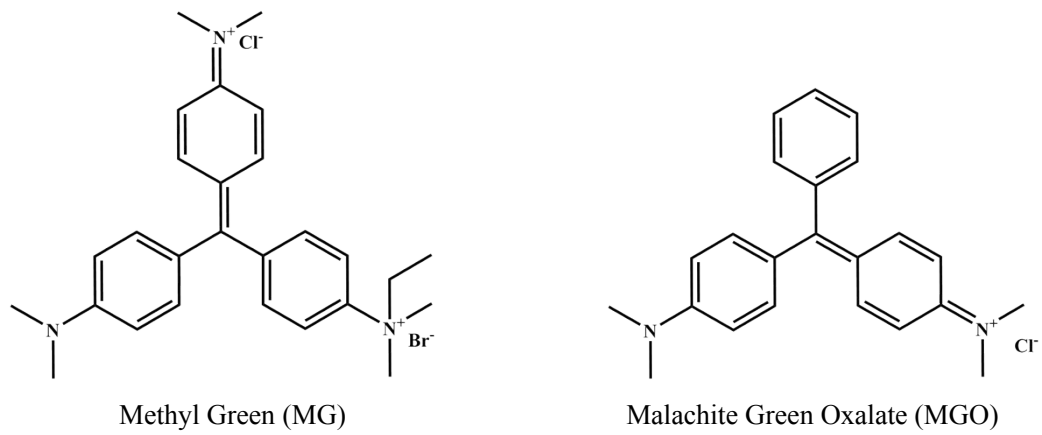


Fig. S11 The structures of three kinds of dyes.

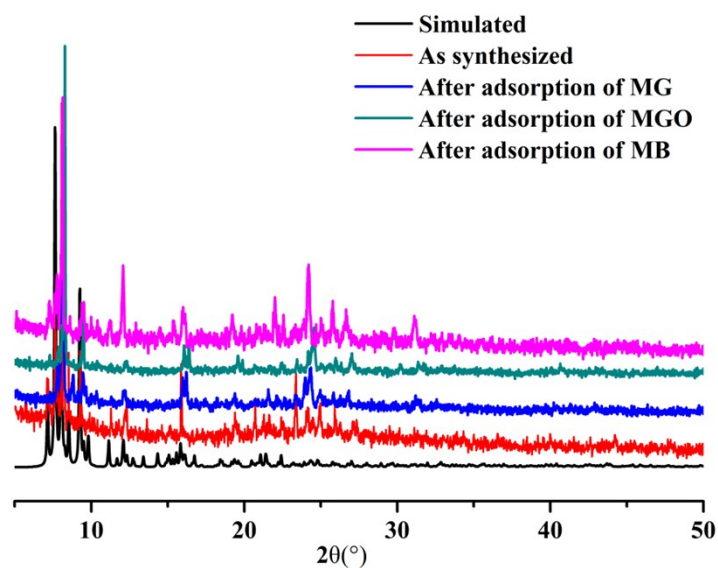


Fig. S12 Stability of MOF 1 for MG, MGO and MB dyes.